Spatiotemporal Variability of the Global Ocean Internal Processes Inferred from Satellite Observations

YANG YANG

School of Marine Sciences, and Center for Ocean-Atmosphere Dynamical Studies, Nanjing University of Information Science and Technology, Nanjing, China

X. SAN LIANG

School of Marine Sciences, School of Atmospheric Sciences, and Center for Ocean-Atmosphere Dynamical Studies, Nanjing University of Information Science and Technology, Nanjing, China

ABSTRACT

Using a new analysis tool, namely, multiscale window transform (MWT), and the MWT-based theory of canonical transfer, this study investigates the spatiotemporal variations of the nonlinear interactions among the mean flows, interannual variabilities, quasi-annual fluctuations, and eddies in the global ocean. It is found that the canonical kinetic energy (KE) transfers are highly inhomogeneous in space, maximized in the western boundary current (WBC), Southern Ocean, and equatorial regions. In contrast to the equatorial and WBC regions where the temporal KE cascades are mainly forward, the Southern Ocean is the very place where coherent large-scale patterns of inverse KE cascade take place. The canonical transfers are also found to be highly variable in time. Specifically, in the Kuroshio Extension, the transfer from the mean flow to the interannual variability is in pace with the external winds from the eastern North Pacific; in the subtropical gyre, the mean flow-to-eddy transfer is responsible for the variability of the eddy kinetic energies (EKE) at both interannual and seasonal scales; in the tropics, the downscale transfers to the eddies from the other three scales all contribute to the interannual modulation of the EKE, and these transfers tend to decrease (increase) during El Niño (La Niña) events. In the Southern Ocean, the high-frequency eddies are found to feed KE to the low-frequency variability through temporal inverse cascade processes, which have been strengthened due to the enhanced eddy activities in the recent decade. Also discussed here is the relation between the seasonal EKE variability and the eddy–quasi-annual fluctuation interaction.

1. Introduction

Oceanic flows are characterized by a broadband of spatial and temporal variabilities. Due to their nonlinear nature, motions on different scales can influence each other through complex interactions, with energy transferred across the scales. Evaluating the interscale energy transfer processes not only improves our understanding of the fundamental problems of oceans such as instabilities, turbulent cascades, and eddy-driven low-frequency variabilities (Scott and Arbic 2007; Tulloch et al. 2011; Aluie et al. 2018; O'Rourke et al. 2018; Sérazin et al. 2018), to name a few, but also makes a basic step toward the construction of energetically consistent ocean models (Eden et al. 2014).

Ever since Lorenz (1955) introduced the theory of energy cycle using Reynolds mean–perturbation decomposition, energetics analysis has become a standard approach in the studies of eddy–mean flow interactions, flow instabilities, and energy cascades in the atmosphere and oceans (Liang and Robinson 2005, 2007; Li et al. 2007; von Storch et al. 2012; Zemskova et al. 2015; Liang 2016; Pan et al. 2017). By probing into the energy pathway between the mean flow and the eddies, it has been well established that baroclinic instability is the main mechanism to generate eddies in the global ocean (Ferrari and Wunsch 2009; von Storch et al. 2012). The energy pathway becomes much more complicated in strong current systems such as the western boundary current (WBC) and the Antarctic Circumpolar Current (ACC) regions because strong barotropic instability may also play a role to transfer energy from the

---

Corresponding author: X. San Liang, x.san.liang@gmail.com

background flow to the eddies (Yang and Liang 2016; Yang et al. 2017; Youngs et al. 2017). In addition, the eddies can also frequently transfer their energy back to the mean flow, such as in the downstream of the Kuroshio Extension (Yang and Liang 2016), reflecting the inhomogeneity of eddy–mean flow interactions in the ocean.

Besides the Lorenz-type energetics, Saltzman (1957) developed an energetics formalism using Fourier transform (hereafter called Saltzman-type formalism). By diagnosing the spectral kinetic energy (KE) flux in the South Pacific Ocean from satellite altimetry measurements, Scott and Wang (2005) found that the oceanic KE is extracted at small spatial scales near the Rossby deformation radius, and transferred back to larger scales through an inverse/upscale KE cascade, consistent with the classical quasi-two-dimensional turbulence theory (e.g., Charney 1971; Salmon 1980). Such inverse KE cascades in the wavenumber space are later confirmed in a vast number of follow-up studies using observations and numerical models in different parts of the World Ocean (Schlösser and Eden 2007; Scott and Arbic 2007; Capet et al. 2008; Klein et al. 2008; Tulloch et al. 2011; Venaille et al. 2011; Wang et al. 2015; Sasaki et al. 2017; Khatri et al. 2018). Recently, Arbic et al. (2012, 2014) extended the spectral analysis to the wavenumber–frequency domains, and demonstrated the existence of a temporal upscale cascade of surface oceanic KE. This temporal inverse cascade, analogs to the well-known spatial inverse cascade, is important in that it may provide a significant internal source for the low-frequency variabilities in the ocean (Berloff et al. 2007; Penduff et al. 2011; O'Rourke et al. 2018; Sérazin et al. 2018).

In a clear and comprehensive way, Liang (2016) established that one of the major issues embedded in the Saltzman-type or Lorenz-type (using Reynolds decomposition) formalisms is that localization is lost in at least one dimension of space–time to achieve scale decomposition. In other words, with these formalisms the resulting energetics cannot simultaneously possess a full spatial structure while retaining its temporal variability. Another important issue in formulating multiscale energetics is how to achieve a physically consistent local expression of interscale energy transfer (Liang 2016). For regional diagnostics, so far there have been in the literature multiple engineering or empirical definitions for the transfer between scales (Holopainen 1978; Plumb 1983; Aluie et al. 2018). This is essentially how to separate the nonlinear advection term in the energy equation into a transfer term, which represents exchanges of energy across scales, and a transport term (in a divergence form), which only redistributes energy in the physical space and hence integrates to zero over a closed domain. Recently, it has been shown that the

previous engineering/empirical formalisms are not physically consistent in energetics as the resulting energy transfers do not conserve. By taking advantage of a new functional analysis tool, namely, multiscale window transform (MWT; Liang and Anderson 2007), Liang (2016) reconstructed an "atomic" energy flux on the multiscale windows and achieved a unique separation of energy transfer from energy transport. The resulting transfer is in a Lie bracket form and satisfies the Jacobian identity, just as the Poisson bracket in Hamiltonian dynamics; for this reason, it has been called "canonical transfer." A canonical transfer sums to zero over scale windows (Liang 2016, p. 4445, Theorem 3.1), indicating that it is simply a redistribution of energy among the scale windows. Just as transport integrates to zero over a closed spatial domain, it must also conserve in the space of scale. This property, though simple to state, does not hold other local Lorenz-type formalisms. [Note that the Saltzman-type formalism, which integrates out all the spatial derivatives, does not have the transport-like term (in divergence form), and hence there is no such problem like the ambiguity in separating transport from transfer, a fundamental problem in Lorenz-type energetics (e.g., Plumb 1983).]

In this study, we present an implementation of the canonical transfer theory to quantify energy transfers between different temporal scales in the global ocean. Distinguished notably from the classical Lorenz-type or Fourier-type formalisms, the canonical transfer is localized in both space and time. In other words, it can be used to diagnose energy cascades at any geographic location and any instant of time. Here we apply the method to a new global total current (the sum of altimetric geostrophic current and modeled Ekman current) synthesis (Rio et al. 2014) to investigate the canonical transfers in the ocean, with an emphasis on their temporal variabilities, which, as far as we know, remain largely unclear.

The rest of the paper is organized as follows. In section 2, we begin with a brief introduction of the canonical transfer theory, and present the observation data used to estimate it. The long-term mean maps of canonical transfers are described in sections 3, and their temporal variabilities are examined in section 4. This study is summarized in section 5.

2. Methodology and dataset

a. Multiscale window transform

As mentioned in the introduction, the classical Lorenz-type formalisms formulated with temporal (or zonal) averaging only result in time-mean (or zonal mean) energetics (e.g., Lorenz 1955; von Storch et al. 2012); they are inappropriate for investigating energy burst

processes, for example, instabilities, which tend to be locally defined in both space and time. A common practice during the past decades is to use filters. However, how multiscale energy should be represented with the filtered fields has become a fundamental problem. For example, a field $f(t)$ may be temporally filtered into a background part $\bar{f}$ and an eddy part f'. If $\bar{f}$ = const is constant, this filtering is simply an averaging, and we know the energies are $\bar{f}^2/2$ and $\overline{f'^2}/2$, respectively, from the Lorenz formalism. However, when both parts are time dependent: $\bar{f} = \bar{f}(t)$, what are the corresponding energies for the background and eddy parts? During the past decades, it has been a common practice to simply set them as $\bar{f}^2/2$ and $f'^2/2$ (i.e., to remove the averaging from $\overline{f'^2}/2$ the Lorenz-type eddy energy). This is, unfortunately, conceptually wrong. To illustrate, suppose f has a simple Fourier expansion with only two frequencies ω_0 and ω_1 ($\omega_0 < \omega_1$):

$$f(t) = \underbrace{(a_0\cos\omega_0 t + b_0\sin\omega_0 t)}_{\bar{f}} + \underbrace{(a_1\cos\omega_1 t + b_1\sin\omega_1 t)}_{f'}.$$

(1)

We know, in the power spectrum, the energies for the two different scales should be $(a_0^2 + b_0^2)/2$ and $(a_1^2 + b_1^2)/2$, respectively, that is, the square of the respective Fourier coefficients, which are phase space variables (independent of t here). They are absolutely not equal to the square of the reconstructed (filtered) fields, that is, $\bar{f}^2/2$ and $f'^2/2$, which are in physical space (functions of t). That is to say, multiscale energy is a concept with the Fourier coefficients in phase space, which is related to its physical space counterpart through the Parseval equality in functional analysis [see Liang (2016) for details]. In Eq. (1), when $\bar{f}$ is a constant, it can be easily proved that $(a_1^2 + b_1^2)/2 = \overline{f'^2}/2$, just as the eddy energy in the Lorenz formalism using the Reynolds decomposition. This explains why the averaging operator in the Lorenz's energetics formalism cannot be removed, otherwise the resulting energy only bears the unit of energy, but does not make any sense in physics.

So it is by no means as trivial a problem as many people have been doing to obtain a physically consistent expression of time-dependent multiscale energy. In fact, this is a rather complex and fundamental problem, and has been an impossible task until filter banks and wavelets are connected (Strang and Nguyen 1996). It has just been systematically addressed by Liang and Anderson (2007) in the development of multiscale window transform (MWT) for this very purpose.

MWT is a functional analysis tool that decomposes a function space into a direct sum of orthogonal subspaces, each with an exclusive range of scales, while preserving its local properties. Such a subspace is called a *scale window*. MWT is developed for a faithful representation of the multiscale energies on the resulting scale windows, in order to make multiscale energetics analysis possible [Liang and Anderson (2007); a brief introduction is referred to in Liang (2016, section 2)]. Liang and Anderson (2007) found that, for some specially constructed orthogonal filters, there exists a transfer–reconstruction pair, namely MWT and its counterpart multiscale window reconstruction (MWR). In some sense MWR functions just like a filter in the traditional sense. What makes it different is that, for each MWR, there exists an MWT that gives coefficients which can be used to represent the energy of the filtered series. In this way multiscale energetics analysis is made possible. In this study, the MWT is applied in the frequency domain. Given a time series $f(t)$, application of the MWT will yield MWT coefficients, which we write as $\hat{f}_n^{\sim\varpi}$, where $\widehat{(\cdot)}_n^{\sim\varpi}$ denotes MWT on window ϖ at time step n, and through MWR we obtain a reconstruction on window ϖ, written as $f^{\sim\varpi}(t)$. By a theorem called the property of marginalization, Liang and Anderson (2007) proved that the energy on window ϖ is proportional to the square of the coefficients $(\hat{f}_n^{\sim\varpi})^2/2$. Note it is by no means as trivial as $[f^{\sim\varpi}(t)]^2$, which has frequently been seen in the literature.

b. Canonical transfer theory

Previous studies have suggested that oceanic processes tend to occur on a range of scales or scale windows, as introduced by Liang and Robinson (2005). In this study, we use the MWT to decompose an oceanic field into persistence and variabilities defined on four scale windows, namely, time-mean flow window, interannual window (with a period longer than 512 days), quasi-annual window (with a period shorter than 512 days and longer than 128 days), and high-frequency transient eddy window (with a period shorter than 128 days). The choice of the cutoff periods are close to those in Penduff et al. (2010). Note that here the cutoff periods are chosen so because, analogous to the wavelet analysis, the number of time steps for scale definition needs to be a power of 2; see Liang (2016) for more details. For easy reference, the four windows are henceforth denoted by $\varpi = 0, 1, 2,$ and 3, respectively.

The interaction between the scale windows is characterized by the energy transfer between them. A faithful representation of the transfer process is hence of key importance. This is addressed in the theory of canonical transfer, which we briefly summarize henceforth. For details, refer to Liang (2016, section 3).

Consider a scaler field T in an incompressible flow $\mathbf{u}$ (here diffusion is neglected for simplicity). It evolves according to the equation

$$\frac{\partial T}{\partial t} + \nabla \cdot (\mathbf{u}T) = 0. \tag{2}$$

Due to the existence of nonlinear advection, multiscale interactions are expected to happen. Take MWT on both sides of Eq. (2) and multiply it by $\hat{T}_n^{\sim\varpi}$, we have the energy equation on window ϖ:

$$\frac{\partial E_n^\varpi}{\partial t} = -\hat{T}_n^{\sim\varpi}\nabla \cdot \widehat{(\mathbf{u}T)}_n^{\sim\varpi}, \tag{3}$$

where $E_n^\varpi = (1/2)(\hat{T}_n^{\sim\varpi})^2$ is the energy on window ϖ at time step n. Note here it is the square of transform coefficient, not the square of some reconstruction or filtered variable, that makes the multiscale energy. Most popular filters used in atmosphere–ocean science do not have such a transform coefficient and hence cannot even allow multiscale energy to be defined.

One continuing effort in multiscale energetics studies is to separate the nonlinear term in Eq. (3), $-\hat{T}_n^{\sim\varpi}\nabla \cdot \widehat{(\mathbf{u}T)}_n^{\sim\varpi}$, into a transport process term $\nabla \cdot \mathbf{Q}_n^\varpi$ and an interscale transfer process term Γ_n^ϖ, that is,

$$-\hat{T}_n^{\sim\varpi}\nabla \cdot \widehat{(\mathbf{u}T)}_n^{\sim\varpi} = -\nabla \cdot \mathbf{Q}_n^\varpi + \Gamma_n^\varpi. \tag{4}$$

As mentioned in the introduction, there exist many empirical forms of transport–transfer separation in the literature, which makes the local interpretation of the transfer process quite ambiguous (Holopainen 1978; Plumb 1983). To tackle this problem, Liang (2016) proved, by integrating "atomic fluxes," the fluxes on the multiscale windows can be rigorously obtained [see Liang (2016) for details], that is,

$$\mathbf{Q}_n^\varpi = \frac{1}{2}\hat{T}_n^{\sim\varpi}\widehat{(\mathbf{u}T)}_n^{\sim\varpi}. \tag{5}$$

Subtracting Eq. (5) from Eq. (4), one can easily obtain the interscale transfer:

$$\Gamma_n^\varpi = \frac{1}{2}[\widehat{(\mathbf{u}T)}_n^{\sim\varpi} \cdot \nabla\hat{T}_n^{\sim\varpi} - \hat{T}_n^{\sim\varpi}\nabla \cdot \widehat{(\mathbf{u}T)}_n^{\sim\varpi}]. \tag{6}$$

Notice that Eq. (6) bears a Lie bracket form that satisfies the Jacobian identity, reminiscent of the Poisson bracket in Hamiltonian mechanics; for this reason, it has been termed "canonical transfer" (Liang 2016). The canonical transfer satisfies a very important property, namely,

$$\sum_\varpi \sum_n \Gamma_n^\varpi = 0; \tag{7}$$

that is, it sums to zero upon summation over all the scale windows and the sampling space, indicating that the it is a mere redistribution of energy among the scale windows, without generating or destroying energy as a whole. This property, which seems to be a natural requirement, however does not hold in other energetics formalisms (Liang 2016).

Equation (6) can be further simplified to a more neat expression:

$$\Gamma_n^\varpi = -E_n^\varpi\nabla \cdot \mathbf{u}_T^\varpi, \tag{8}$$

where

$$\mathbf{u}_T^\varpi = \frac{\widehat{(\mathbf{u}T)}_n^{\sim\varpi}}{\hat{T}_n^{\sim\varpi}} \tag{9}$$

has been referred to as the T-coupled velocity. Note that E_n^ϖ is the energy on window ϖ at step n and is, hence, always positive. The sign of the canonical transfer on window ϖ is, therefore, determined by the convergence of the T-coupled velocity.

From the primitive equations, one can derive the KE budget equation on scale window ϖ:

$$\frac{\partial K^\varpi}{\partial t} = \underbrace{-\nabla \cdot \left[\frac{1}{2}\widehat{(\mathbf{u}\mathbf{u}_h)}^{\sim\varpi} \cdot \hat{\mathbf{u}}_h^{\sim\varpi}\right]}_{\nabla \cdot \mathbf{Q}_K^\varpi} \underbrace{-\nabla \cdot \left(\frac{1}{\rho_0}\hat{\mathbf{u}}^{\sim\varpi}\hat{p}^{\sim\varpi}\right)}_{\nabla \cdot \mathbf{Q}_P^\varpi}$$
$$+ \underbrace{\frac{1}{2}\left[\widehat{(\mathbf{u}\mathbf{u}_h)}^{\sim\varpi} : \nabla\hat{\mathbf{u}}_h^{\sim\varpi} - \nabla \cdot \widehat{(\mathbf{u}\mathbf{u}_h)}^{\sim\varpi} \cdot \hat{\mathbf{u}}_h^{\sim\varpi}\right]}_{\Gamma_K^\varpi}$$
$$- \underbrace{\frac{g}{\rho_0}\hat{\rho}^{\sim\varpi}\hat{w}^{\sim\varpi}}_{-b^\varpi} + F_K^\varpi. \tag{10}$$

A detailed derivation is referred to Liang (2016). Here, $\mathbf{u}_h$ is the horizontal velocity vector, ρ_0 the constant reference density, and $K^\varpi = (1/2)\hat{\mathbf{u}}_h^{\sim\varpi} \cdot \hat{\mathbf{u}}_h^{\sim\varpi}$ the KE on window ϖ. The operator (:) represents colon product of two dyads (cf. Liang 2016) such that, for four vectors $\mathbf{A}$, $\mathbf{B}$, $\mathbf{C}$, and $\mathbf{D}$,

$$(\mathbf{A}\mathbf{B}) : (\mathbf{C}\mathbf{D}) = (\mathbf{A} \cdot \mathbf{C})(\mathbf{B} \cdot \mathbf{D}). \tag{11}$$

The other notations are conventional. Note here the time step n has been suppressed for notational simplicity. In Eq. (10), $\nabla \cdot \mathbf{Q}_K^\varpi$ represents the spatial transport of KE by advection on window ϖ, $\nabla \cdot \mathbf{Q}_K^\varpi$ is the pressure work term, b^ϖ denotes the buoyancy conversion between the available potential energy (APE) and KE on window ϖ, and F_K^ϖ denotes the forcing/dissipation processes, which are not explicitly expressed here. Here, Γ_K^ϖ is the canonical transfer term that measures KE transferred from other windows to window ϖ. Since no spatial or temporal averaging are taken, Γ_K^ϖ can faithfully represent the energy cascade
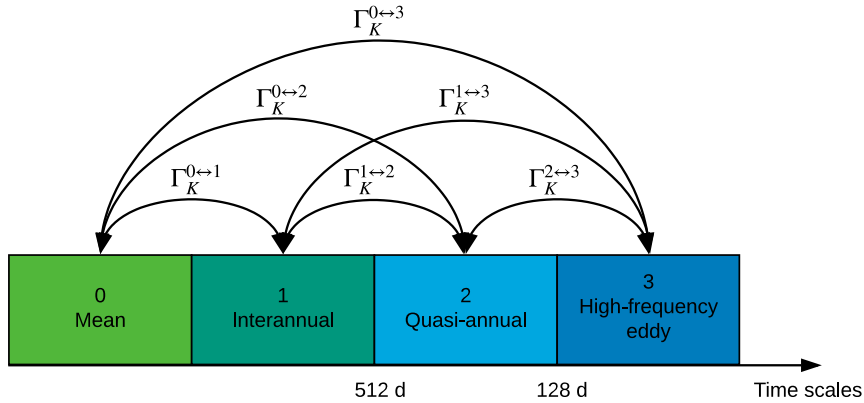
FIG. 1. A schematic of the scale window setting and canonical transfers between different windows. The numbers 0, 1, 2, and 3 stand for the mean flow, interannual, quasi-annual, and eddy windows, respectively.

processes between oceanic motions that are localized and intermittent in space and time.

Note a canonical transfer to a window may involve contributions from different sources. Take the eddy window ($\varpi = 3$) for example: the energy can be from window 0, window 1, window 2, and even from the other different locations (the sampling space) within the same window. Therefore, a technique named "interaction analysis" needs to be further applied in order to select out the window–window interactions.

As shown in Eq. (6), the canonical transfer can be written as a linear combination of terms in the form

$$\Gamma_n^{\varpi} = \hat{\Re}_n^{\sim \varpi} \widehat{(pq)}_n^{\sim \varpi}.$$

It therefore suffices to analyze this single term. Take Γ_n^3, for example:

$$
\begin{aligned}
\Gamma_n^3 = \hat{\Re}_n^{\sim 1} \widehat{(pq)}_n^{\sim 3} &= \hat{\Re}_n^{\sim 3} \overline{\left(\sum_{\varpi_1=0}^{3} p \sum_{\varpi_2=0}^{3} q \right)}_n^{\sim 3} \\
&= \hat{\Re}_n^{\sim 3} \left[\widehat{(p^{\sim 0} q^{\sim 0})}_n^{\sim 3} + \widehat{(p^{\sim 0} q^{\sim 3})}_n^{\sim 3} + \widehat{(p^{\sim 3} q^{\sim 0})}_n^{\sim 3} \right] \\
&+ \hat{\Re}_n^{\sim 3} \left[\widehat{(p^{\sim 1} q^{\sim 1})}_n^{\sim 3} + \widehat{(p^{\sim 1} q^{\sim 3})}_n^{\sim 3} + \widehat{(p^{\sim 3} q^{\sim 1})}_n^{\sim 3} \right] \\
&+ \hat{\Re}_n^{\sim 3} \left[\widehat{(p^{\sim 2} q^{\sim 2})}_n^{\sim 3} + \widehat{(p^{\sim 2} q^{\sim 3})}_n^{\sim 3} + \widehat{(p^{\sim 3} q^{\sim 2})}_n^{\sim 3} \right] \\
&+ \hat{\Re}_n^{\sim 3} \left[\widehat{(p^{\sim 0} q^{\sim 1})}_n^{\sim 3} + \widehat{(p^{\sim 1} q^{\sim 0})}_n^{\sim 3} \right] \\
&+ \hat{\Re}_n^{\sim 3} \left[\widehat{(p^{\sim 0} q^{\sim 2})}_n^{\sim 3} + \widehat{(p^{\sim 2} q^{\sim 0})}_n^{\sim 3} \right] \\
&+ \hat{\Re}_n^{\sim 3} \left[\widehat{(p^{\sim 1} q^{\sim 2})}_n^{\sim 3} + \widehat{(p^{\sim 2} q^{\sim 1})}_n^{\sim 3} \right] \\
&+ \hat{\Re}_n^{\sim 3} \widehat{(p^{\sim 3} q^{\sim 3})}_n^{\sim 3}.
\end{aligned}
\tag{12}
$$

The first three terms on the right-hand side of Eq. (12) represent the energy transfer to window 3 from window 0, 1, and 2, respectively; write them as $\Gamma_n^{0 \to 3}$, $\Gamma_n^{1 \to 3}$, and $\Gamma_n^{2 \to 3}$. Two different scale windows may also combine to contribute to Γ_n^3, though generally the contribution is negligible; these make the fourth to sixth terms. The last term is the transfer from window 3 itself. More details about the interaction analysis can be found in Liang and Robinson (2005, section 9). For the canonical transfers to the other scale windows, see Fig. 1 for illustration.

As is well known in geophysical fluid dynamics, barotropic and baroclinic instabilities can be quantitatively described by the interscale transfers of the KE and APE between the mean flow and the fluctuations, respectively (Pedlosky 1987). Note that a common statement that barotropic and baroclinic instability are, respectively, related to the horizontal and vertical shear of the mean flow is consistent with the concepts of cross-scale energy transfer used in this study. In fact, the former is just a particular case of the latter under quasigeostrophic assumption thanks to the thermal wind relation [see Liang and Robinson (2007) for details]. As we mentioned earlier, the classical transfer formalisms do not conserve energy in the space of scale. In other words, those transfers also contain transports which are irrelevant to hydrodynamic stability. As established by Liang and Robinson (2007), the canonical transfers of the KE and APE correspond precisely to the barotropic instability and baroclinic instability, respectively, in the classical sense in, say, Pedlosky (1987). In Liang and Robinson (2007), they also illustrated, for a benchmark barotropic instability model whose instability structure is analytically known, the traditional transfer does not give the correct source of instability, while canonical transfer does.

c. A new global surface current synthesis

We use a new global surface current synthesis distributed by Copernicus Marine and Environment Monitoring Service (CMEMS) to estimate the canonical

transfer matrices. The gridded ocean current data, with a spatial resolution of $0.25° \times 0.25°$, is obtained by combining the altimeter-derived geostrophic velocities and modeled Ekman currents using ECMWF ERA-Interim wind stress (Rio et al. 2014). Compared to other existing observed products, the advantage of the Copernicus surface current estimation is that, by using information from surface drifters and Argo floats, it constructs a new global mean dynamic topography (i.e., CNES-CLS13 MDT) which resolves spatial scales beyond the resolution permitted by the state-of-the-art geoid models based on GRACE and GOCE data. In addition, a new empirical Ekman model with the joint use of Argo floats and SVP drifters is employed to estimate the ageostrophic Ekman currents in the global ocean. The combining of these two features shows improved estimation of the ocean surface currents (Rio et al. 2014; Pujol et al. 2016). A more thorough description of the dataset is available in Rio et al. (2014). In this study, the surface daily zonal and meridional velocity fields from 1993 to 2016 are used.

3. Spatial characteristics of canonical transfers

a. Global pattern

Figure 2 shows the global patterns of KE on the four scale windows averaged over the 1994–2015 period. The first and last years (i.e., 1993 and 2016) are excluded just in case the boundary influences of MWT might arise. A general observation is that all KE components are inhomogeneous in space, with their maxima mainly concentrated in the vicinity of the WBCs, the Southern Ocean, and the equatorial regions, where background currents are strong. The geographical correspondence to these KE components in different frequency bands suggests that the intense variabilities in these regions may arise from hydrodynamic instabilities of the large-scale mean flows which transfer energy forward across all scales (Williams et al. 2007; Ferrari and Wunsch 2009). The zonally averaged KE components are displayed as a function of latitude in Fig. 3a. It can be seen that the high-frequency eddy KE (EKE; K^3) is the largest reservoir at most latitudes, except in the 45°–55°S band, where the magnitude of the mean KE (K^0) is much larger than other components due to the existence of the Antarctic Circumpolar Current (ACC). The interannual and quasi-annual variabilities, usually regarded as low-frequency variabilities in the ocean, are two important components in the KE spectra (see K^1 and K^2 in Figs. 2b,c and Fig. 3a). Whether such low-frequency variability in the ocean is intrinsically generated or externally excited is still a topic of ongoing research (Penduff et al. 2011; Arbic et al. 2014; O'Rourke et al. 2018;
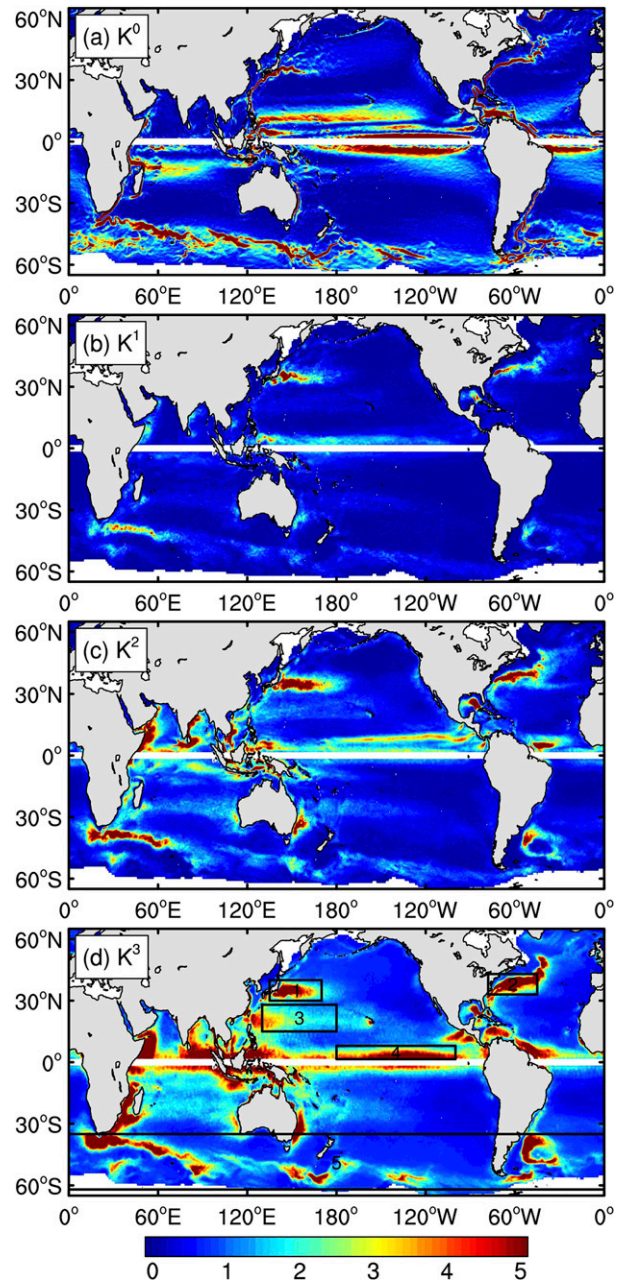

FIG. 2. The long-term mean (1994–2016) maps of KE on (a) the mean flow window (K^0), (b) the interannual window (K^1), (c) the quasi-annual window (K^2), and (d) the eddy window (K^3). Regions within 1.5° of the equator are excluded due to a large bias that may arise in the estimation of the altimeter-derived geostrophic velocities at the equator. The five boxes, marked as 1–5, respectively, represent the five focus regions as explained in the text. The units of the energy components are all in $10^{-2}\,\mathrm{m^2\,s^{-2}}$.

Sérazin et al. 2018). A possible scenario will be discussed in section 4, where the relation between the intrinsic canonical transfer and atmosphere forcing is examined in the Kuroshio Extension region.
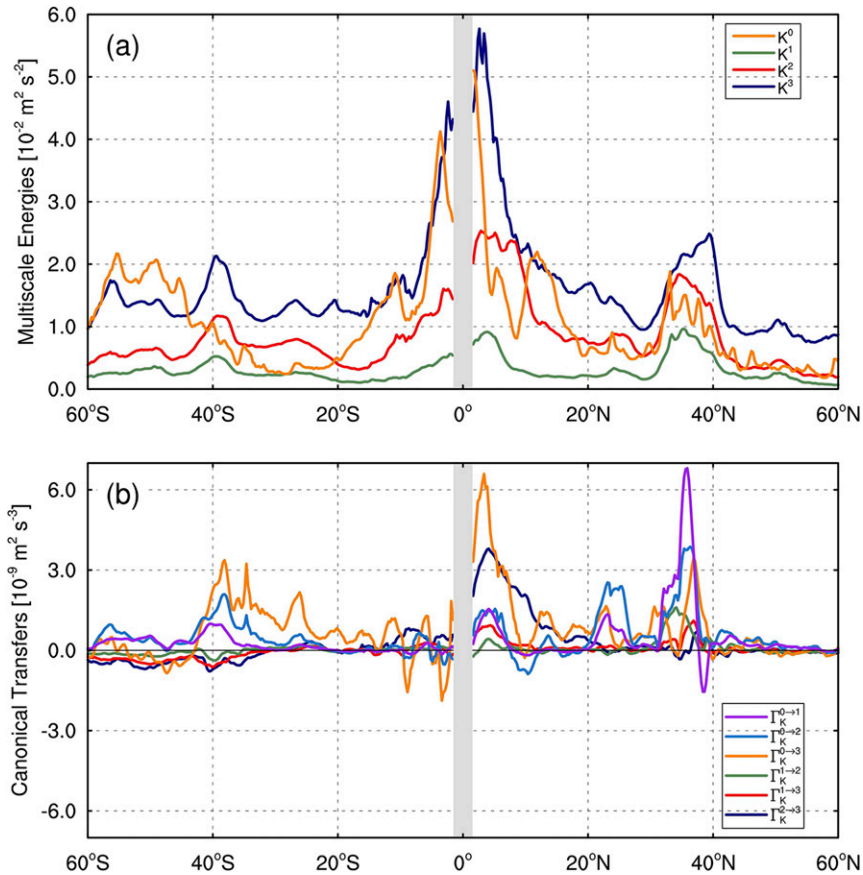
FIG. 3. Zonal average of (a) the multiscale KE components (10^{-2} m^2 s^{-2}) and (b) the canonical transfers (10^{-9} m^2 s^{-3}).

As introduced in section 2, the interaction analysis enables us to investigate the mutual energy transfers among scale windows. Figures 4 and 5 display the long-term mean maps of the canonical transfer matrices, which are dominated by large values in the WBCs, the Southern Ocean and the equatorial regions. Generally, the patterns of these interscale transfers vary substantially from region to region, implying the inhomogeneous nature of multiscale interactions in the ocean.

The interactions between the mean flow and fluctuations in various frequency bands (i.e., $\Gamma_K^{0\to1}$, $\Gamma_K^{0\to2}$, and $\Gamma_K^{0\to3}$) are first analyzed. Figures 4a–c show the spatial patterns of the canonical transfers from the mean flow window to the interannual ($\Gamma_K^{0\to1}$), quasi-annual ($\Gamma_K^{0\to2}$), and eddy ($\Gamma_K^{0\to3}$) windows, respectively. One of the most conspicuous features is the overwhelming positive values in strong current regions, such as the Kuroshio and Gulf Stream Extensions, the Southern Ocean, and the equatorial regions. This implies that the mean flow loses KE to the three frequency bands through barotropic instability, leading to the anomalously high multiscale KEs in these regions. Some regional patterns are also

intriguing. For instance, the $\Gamma_K^{0\to3}$ map clearly reveals a downscale transfer in the upstream Kuroshio Extension and an upscale transfer in the downstream, which has been also documented in previous studies (e.g., Yang and Liang 2016, 2018). In the equatorial region, the barotropically unstable zonal flows are found to provide large amounts of KE to the time-varying fluctuations, particularly to the high-frequency eddies (Fig. 4c). It is interesting to note that significant KE is transferred from the eddies back to the mean flow in many spots in the Southern Ocean, particularly in the Indian and Atlantic Ocean sectors (Fig. 4c), indicating that the eddies act to drive the mean flow in these regions. Similar phenomenon in the Southern Ocean has also been identified in several previous studies (e.g., Wilkin and Morrow 1994). Also note that positive $\Gamma_K^{0\to3}$ occurs in the subtropical gyres of all ocean basins, but with relatively small amplitude compared to that in strong current regions. This suggests that barotropic instability also plays some role in modulating the eddy variability in the subtropical gyres, although its contribution may be secondary compared to the well accepted baroclinic instability as identified in
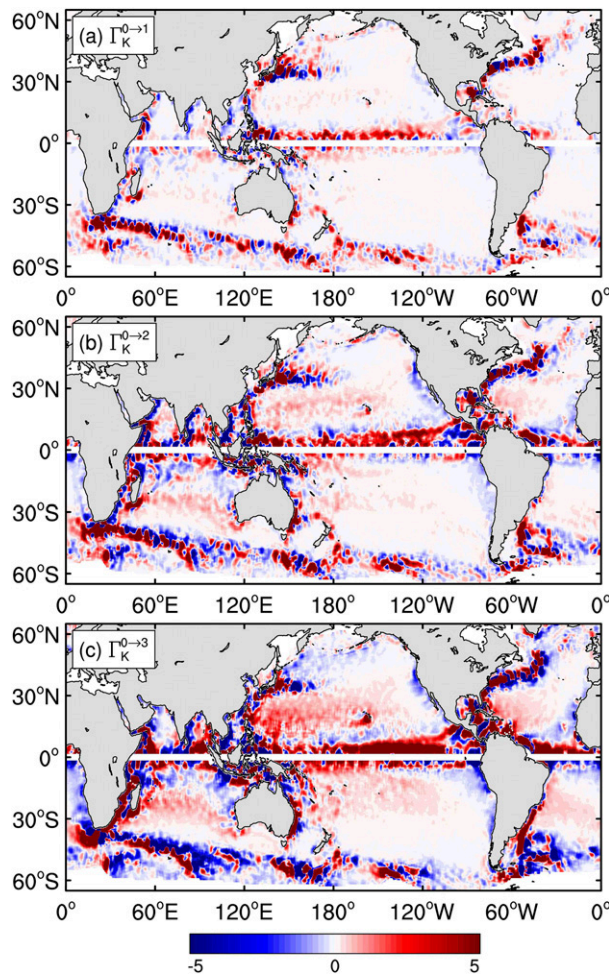
FIG. 4. The long-term mean (1994–2016) maps of (a) $\Gamma_K^{0\to1}$, (b) $\Gamma_K^{0\to2}$, and (c) $\Gamma_K^{0\to3}$. All maps are horizontally smoothed using a 3° running filter. The units of the transfer terms are all in $10^{-9}\,\mathrm{m^2\,s^{-3}}$.

FIG. 5. As in Fig. 4, but for (a) $\Gamma_K^{1\to2}$, (b) $\Gamma_K^{1\to3}$, and (c) $\Gamma_K^{2\to3}$.

previous studies (e.g., Kobashi and Kawamura 2002; Chang and Oey 2014).

Figure 5 shows the distributions of the canonical transfers among the interannual, quasi-annual and eddy windows. Generally, these terms are smaller in magnitude than the mean flow-related ones, and the sign of them displays large spatial variations. In the WBC regions such as the Kuroshio and Gulf Stream Extensions, although mingled with negative patches, the canonical transfers from the interannual fluctuations to the quasi-annual ($\Gamma_K^{1\to2}$) and to the eddy ($\Gamma_K^{1\to3}$) variabilities are mostly positive, indicating that the direction of the temporal KE cascades is mainly downscale in these regions. In contrast, the Southern Ocean is characterized by strong negative $\Gamma_K^{1\to2}$ and $\Gamma_K^{1\to3}$ (Figs. 5a,b), which means that inverse KE cascades from the quasi-annual and transient eddies are intrinsic energy sources for the interannual variability in this region. Figure 5c shows the KE transfer from the
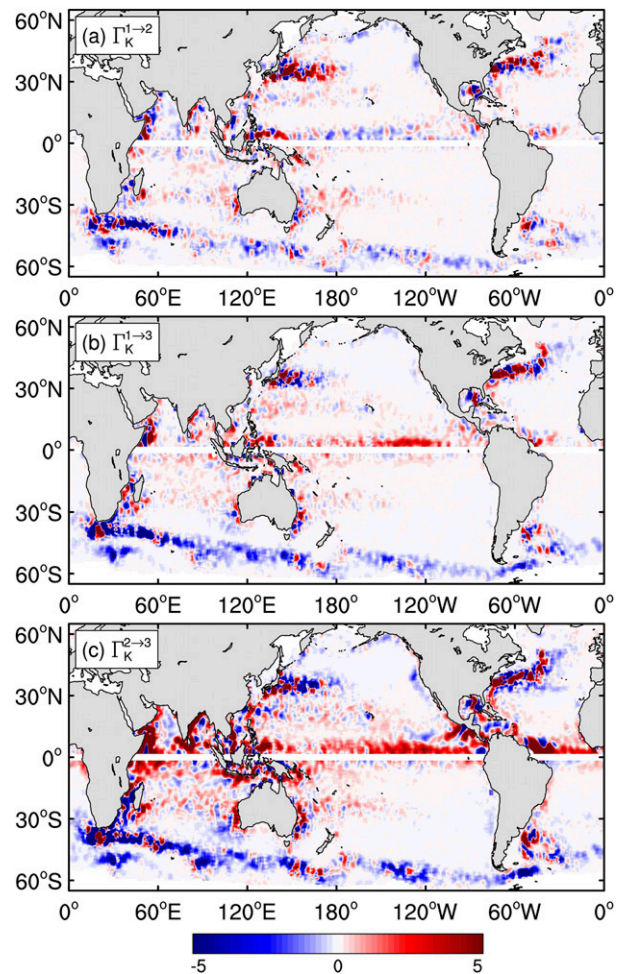
quasi-annual fluctuations to the high-frequency eddies ($\Gamma_K^{2\to3}$), which exhibits strong negative values in the Southern Ocean and positive values in the tropical regions. In the WBC regions such as the Kuroshio and Gulf Stream Extensions, the quasi-annual fluctuation–eddy interactions exhibit rather complex horizontal patterns. For instance, the quasi-annual fluctuation loses KE to the eddies in the upstream Kuroshio Extension region, while gaining KE from the eddies in the downstream region.

Figure 3b further illustrates the meridional variation of the canonical transfer terms. The zonally averaged transfers reach their maxima around the midlatitude and tropical bands, corresponding to the high KE reservoirs in these bands. It can be seen that the mean flow releases KE to the three frequency bands at most latitudes. Significant inverse energy cascades are found south of 30°S, while forward cascades mainly occur in the tropical and midlatitude bands in the Northern Hemisphere.

Previous studies have used the Fourier-type method to examine the spectral transfers in the frequency

domain (Arbic et al. 2012, 2014; O'Rourke et al. 2018; Sérazin et al. 2018). For instance, with a realistic ocean model and satellite altimeter products Arbic et al. (2014) suggested that the nonlinear interaction can drive intrinsic low-frequency variability through a "temporal inverse cascade," analogs to the well-known spatial inverse cascade in geostrophic turbulence. It should be pointed out that our canonical transfer [see Eq. (10)] is fundamentally different from the traditional ones. As illustrated in section 2, the canonical transfer describes nonlinear interactions that only act to transfer energy among scales, which excludes the spatial transport processes embedded in nonlinearly intertwined energetics (Liang 2016). Such property is not met or even considered in previous formalisms. From the global maps of the long-term mean canonical transfers, we can see that temporal inverse KE cascades, or the so-called eddy-driven low frequency variability, do not take place everywhere in the ocean. Surprisingly, our results show that the Southern Ocean is the very place where coherent large-scale pattern of inverse cascades take place, while at the high latitudes in the Northern Hemisphere, the KE cascades are overall downscale in direction.

b. Regional routes

From the previous subsection, we learned that the direction and magnitude of the KE cascade differ strongly in space. In this section, we select five typical regions where strong eddy variabilities occur, that is, the Kuroshio Extension (30°–40°N, 135°–170°E), the Gulf Stream (33°–43°N, 78°–45°W), the North Pacific subtropical gyre (15°–28°N, 130°W–180°), the tropical Pacific (1.5°–8°N, 180°–100°W), and the Southern Ocean (62°–35°S), to investigate the regional variations of the canonical transfers. These five regions are marked and labeled by numbers in Fig. 2d. The domain-averaged transfer rates are summarized in Table 1. An important feature we observe in Table 1 is that the directions of the KE transfers are mostly downscale in these selected regions. One exception is the Southern Ocean, where strong and significant upscale canonical transfers take place, distinctly different from the WBCs and their extension regions. This phenomenon suggests that the dynamics of the Southern Ocean might be quite different from that of the WBC systems. As is well known in turbulence theory, in a homogeneous, isotropic 3D turbulence, the nonlinear interaction tends to transfer KE from large to small scales, while in a 2D or quasi-geostrophic system, KE is expected to cascade from small to large scales (e.g., Salmon 1980; Scott and Wang 2005). According to the simple Taylor (1938) hypothesis that relating the frequency and wavenumber of a turbulent flow, the distinct features of the temporal KE cascade

TABLE 1. Long-term mean of the canonical transfers averaged over the five focus regions and the global ocean. Values are in $10^{-9}\,\mathrm{m^2\,s^{-3}}$.

	$\Gamma_K^{0\to1}$	$\Gamma_K^{0\to2}$	$\Gamma_K^{0\to3}$	$\Gamma_K^{1\to2}$	$\Gamma_K^{1\to3}$	$\Gamma_K^{2\to3}$
Kuroshio Extension	7.22	4.61	1.45	3.41	0.72	−0.27
Gulf Stream	3.43	5.04	4.32	0.85	1.32	1.53
Subtropical gyre	0.09	0.37	1.04	0.05	0.17	0.09
Tropical Pacific	1.07	1.84	9.53	−0.25	0.94	1.78
Southern Ocean	0.42	0.68	0.49	−0.14	−0.36	−0.46
Global ocean	0.34	0.48	0.82	0.04	0	0.31

in the Southern Ocean and the WBC system may suggest that the Southern Ocean is more like a 2D turbulent flow, while the dynamics of the WBCs such as Kuroshio and Gulf Stream Extensions are more 3D. It must be noted that, however, the Taylor hypothesis might not hold precisely in the real ocean (Arbic et al. 2014), and, therefore, caution should be used here.

The domain averages of the mean flow-related canonical transfers (i.e., $\Gamma_K^{0\to1}$, $\Gamma_K^{0\to2}$, and $\Gamma_K^{0\to3}$) exhibit positive signs in all the chosen regions, indicating that the mean flow loses KE to the three frequency bands via barotropic instability. In the Kuroshio Extension region, we observe that the high-frequency eddies gain energy from the interannual-scale variability (positive $\Gamma_K^{1\to3}$) and lose energy to the quasi-annual-scale variability (negative $\Gamma_K^{2\to3}$). From the horizontal pattern shown in the previous subsection, we learned that the upscale transfer is mostly distributed in the downstream region of the Kuroshio Extension (Fig. 5c). In the tropical Pacific, the direction of all these cross-scale transfers is forward except $\Gamma_K^{1\to2}$, which shows a relatively weak inverse transfer from the quasi-annual motions to the interannual fluctuations.

Intrinsic low-frequency variability is of wide concern in understanding the climate system. We have found that the temporal inverse cascade does not take place everywhere in the ocean. In fact, in ocean domains such as the WBC regions, the interannual KE mainly comes from the barotropic instability of the mean flow (i.e., $\Gamma_K^{0\to1}$), rather than inverse cascade from high-frequency motions. Even in the Southern Ocean, the contribution to the interannual KE from the mean flow through downscale canonical transfer and that from high-frequency motions through upscale canonical transfer is comparable. When averaging over the global ocean, all the canonical transfers exhibit positive values except $\Gamma_K^{1\to3}$, whose global mean is negligible compared to other terms.

4. Temporal variations of the canonical transfers

The multiscale energetics diagnosis has been widely used to investigate ocean turbulence. However, the
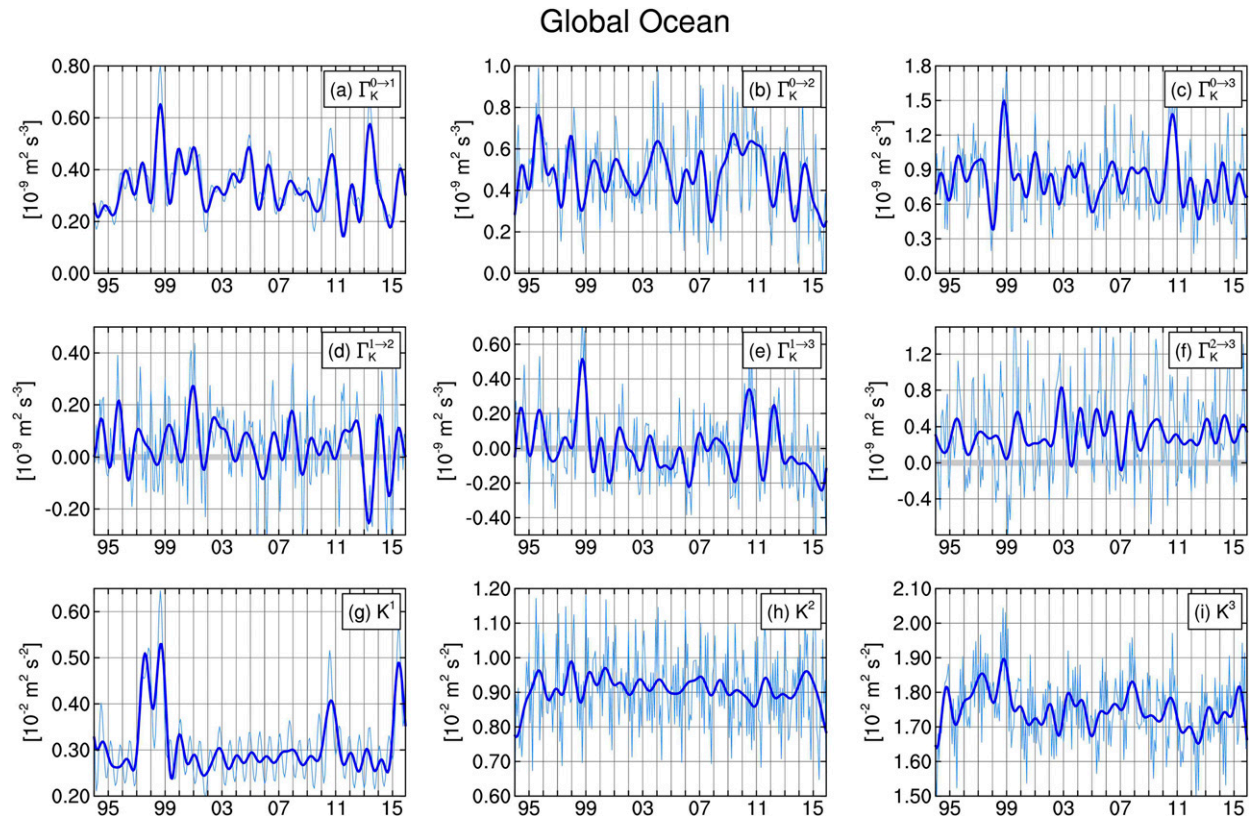
Global Ocean

FIG. 6. Time series of (a)–(f) canonical transfers (10^{-9} m^2 s^{-3}) and (g)–(i) multiscale KEs (10^{-2} m^2 s^{-2}) averaged over the global ocean (65°S–65°N).

temporal variations of the energetics have not yet been well explored. Considering that energy transfer processes across different scales substantially control the energy budget, evaluating the temporal changes of these interactions are very important for a better understanding of the multiscale variabilities of the ocean motions (e.g., Stammer and Wunsch 1999). This section examines the temporal variabilities of the canonical transfers in the ocean. Also discussed is to what degree are these energy cascade processes related to the associated multiscale KEs as well as certain climate modes.

a. Interannual modulation and trend

Figure 6 shows the time series of the globally averaged canonical transfers and multiscale KEs during the period of 1994–2016, from which we have two general observations. First, from a global mean perspective, the signs of the canonical transfers from the mean flow window to the interannual, quasi-annual, and eddy windows are always positive (Figs. 6a–c), consistent with the barotropic instability pathway in the upper ocean (von Storch et al. 2012), even though their magnitudes change from time to time. Second, the global-mean

transfers among the interannual, quasi-annual, and eddy windows exhibit significant high-frequency oscillation as well as low-frequency modulation (Figs. 6d–f). Compared to the mean-flow-related transfers, these terms change their signs constantly, reflecting the complex nature of multiscale interactions in the ocean. Considering that the distributions of canonical transfers are highly inhomogeneous (see Figs. 4 and 5), we will focus on the temporal variability of these transfer processes in the following selected regions.

The low-frequency (interannual to decadal) variability in the Kuroshio Extension region has caught much attention during the past decade. Whether such low-frequency oscillation is purely intrinsic or externally forced is still under debate (Qiu 2003; Taguchi et al. 2007; Pierini 2014; Yang et al. 2017). Figures 7a and 7b show the time series of $\Gamma_K^{0 \to 1}$ and K^1, respectively, averaged over the Kuroshio Extension region. Enhanced interannual variabilities are detected in 1999–2008, whereas low interannual variabilities are observed in 1994–98 and 2009–16. The interannual-scale KE is found to be positively correlated with the canonical transfer $\Gamma_K^{0 \to 1}$ with no evident time lag (correlation coefficient $r = 0.82$; Fig. 7d), indicating that barotropic instability,
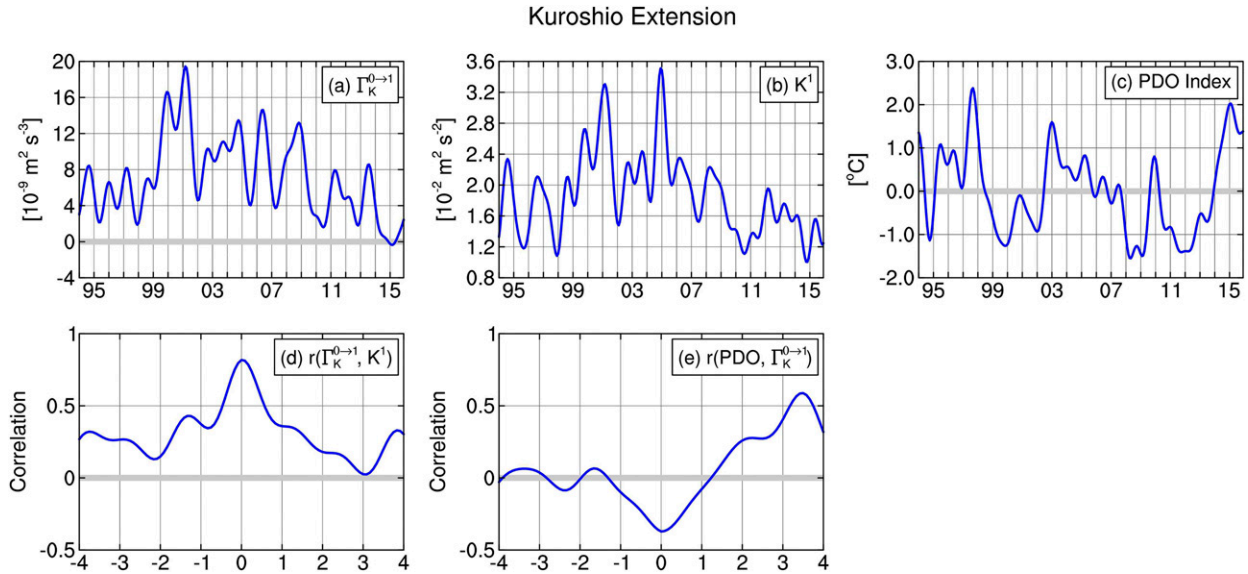
Kuroshio Extension

FIG. 7. Time series of (a) $\Gamma_K^{0\to1}$ (10^{-9} m^2 s^{-3}), (b) K^1 (10^{-2} m^2 s^{-2}) averaged over the Kuroshio Extension region, and (c) the low-pass (longer than 13 months) filtered Pacific decadal oscillation (PDO) index. (d) Lag correlation between the $\Gamma_K^{0\to1}$ and the K^1 time series. A positive lag indicates that $\Gamma_K^{0\to1}$ takes the lead. (e) Lag correlation between the PDO index and the $\Gamma_K^{0\to1}$ time series. A positive lag indicates that the PDO index takes the lead.

which acts to extract KE from the mean flow to the interannual-scale variability, is responsible for the low-frequency variability in this region. During the past decade, it has been well established that the large-scale sea level variability in the Kuroshio Extension region can be explained by the westward propagation of baroclinic Rossby waves which are generated by the PDO-related wind forcing in the eastern North Pacific with a delay of 3–4 years (Qiu 2003). Here we show that the $\Gamma_K^{0\to1}$ is also positively correlated with the PDO index, with a correlation coefficient of 0.59 when the PDO leads $\Gamma_K^{0\to1}$ by about 3.5 years (Fig. 7e). This suggests that the Kuroshio Extension's internal oscillation could be possibly triggered by the external forcings from the eastern North Pacific.

Significant interannual-to-decadal eddy variabilities are observed in the North Pacific subtropical gyre. Baroclinic instability has been considered as the main mechanism that controls such low-frequency EKE modulation (Qiu and Chen 2013; Chang and Oey 2014). Figures 8a and 8b show the low-pass-filtered time series of the canonical transfer from the mean flow to the eddies ($\Gamma_K^{0\to3}$) and EKE (K^3), respectively. Interestingly, these two series are highly correlated with a correlation coefficient of 0.87 (Fig. 8d), indicating that barotropic instability is also responsible for the low-frequency modulation of the eddy activities in the subtropical gyre region, although its contribution might be secondary compared to baroclinic instability as suggested by previous investigators (e.g., Chang and Oey 2014).

In addition, $\Gamma_K^{0\to3}$ is found to lag behind the PDO index by about 6 months (Fig. 8e), seemingly in agreement with the time period adjusting to the PDO-related surface forcing (Qiu and Chen 2013).

In section 3, we found that strong forward KE cascades occur in the tropical ocean in a long-term mean sense. Here we further examine the temporal variability of these cascade processes. Figures 9a and 9b show the time series of the eddy-related canonical transfers (i.e., $\Gamma_K^{0\to3}$, $\Gamma_K^{1\to3}$, and $\Gamma_K^{2\to3}$) and EKE averaged in the North Pacific tropical region, respectively. The high correlation between the EKE and all three transfers (Fig. 9d) demonstrates that the high-frequency eddy motions not only extracts KE from the mean flow, but also receives energy from the interannual as well as the quasi-annual scale variabilities. It is also noted that the correlation between the changes in ocean energetics and that in sea surface temperature is negative at zero lag (Fig. 9e), and such relation is particularly evident during 1997–2000 and 2009–11 when a strong El Niño followed by a strong La Niña occurs (Fig. 9a,e), indicating that the forward KE cascades decrease (increase) during El Niño (La Niña) events. These finding are consistent with the study of Zheng et al. (2016), who found that the number of tropical instability vortices (TIVs) during El Niño events is much lower than that during the subsequent La Niña events in the eastern tropical Pacific Ocean.

The transient EKE field in the Southern Ocean exhibits strong interannual variability (Fig. 10d); it is well
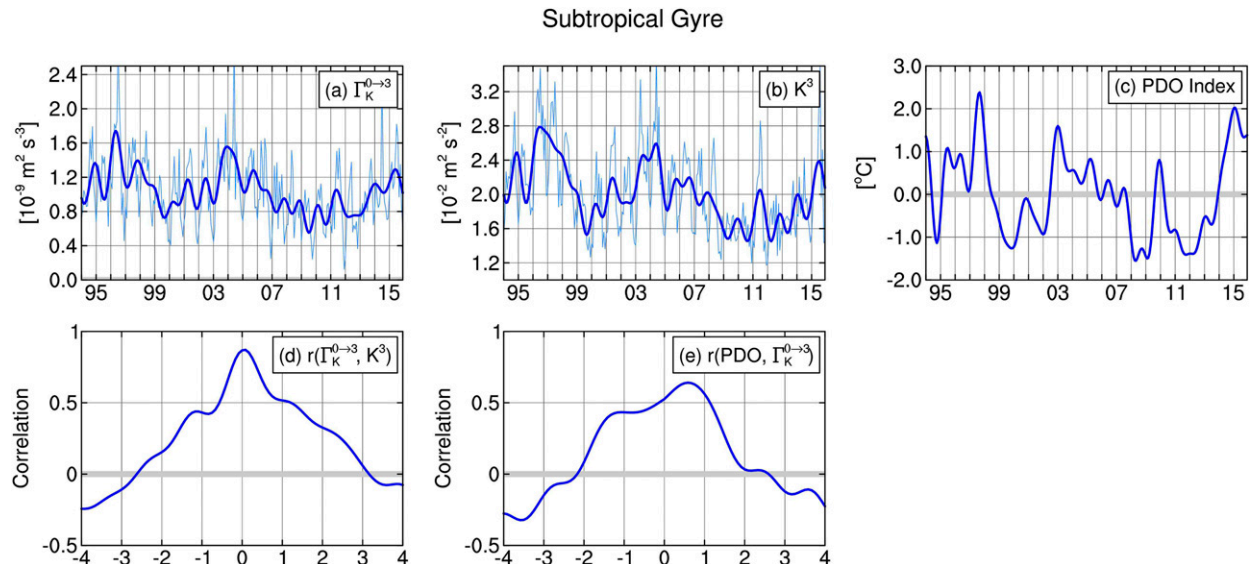
Subtropical Gyre

FIG. 8. Time series of (a) $\Gamma_K^{0\to3}$ ($10^{-9}\,\mathrm{m^2\,s^{-3}}$), (b) K^3 ($10^{-2}\,\mathrm{m^2\,s^{-2}}$) averaged over the North Pacific subtropical gyre region, and (c) the low-pass-filtered PDO index. In (a) and (b), thin lines indicate the original time series and thick lines denote the time series after a low-pass filtering that has a cutoff period of 13 months. (d) Lag correlation between the $\Gamma_K^{0\to3}$ and the K^3 time series. A positive lag indicates that $\Gamma_K^{0\to3}$ takes the lead. (e) Lag correlation between the PDO index and the $\Gamma_K^{0\to3}$ time series. A positive lag indicates that the PDO index takes the lead.

correlated with the interannual variations of the wind stress with a lag of 2–3 years (Meredith and Hogg 2006). Figures 10a–c show the canonical KE transfers to the eddies from the mean flow, interannual, and quasi-annual scale variability in this region, respectively. No significant correlation is found between the EKE and these canonical transfers at interannual time scale (not shown). In addition to the interannual variability, a significant increasing trend of EKE is observed in the Southern Ocean (Fig. 10d). As evidenced in Fig. 10a, $\Gamma_K^{0\to3}$ exhibits a decreasing trend in the recent decades (note the positive sign). This implies that barotropic instability is not responsible for the increasing EKE trend in this region. Using idealized high-resolution ocean models, Hogg et al. (2015) suggested that the recent trend in EKE is most likely due to continuing increases in the wind stress over the Southern Ocean. Interestingly, there exists a clear decreasing trend of $\Gamma_K^{1\to3}$ (note the negative sign) as depicted in Fig. 10b. This implies that the eddies acts to supply KE for the interannual variability through temporal inverse cascade processes, and such cascade processes get strengthened due to the enhanced eddy activities in the recent decade. Similar trend is also found in $\Gamma_K^{2\to3}$ (Fig. 10c), suggesting the important role played by the upscale feedback processes from the transient eddies in the Southern Ocean.

b. Seasonality

Thanks to the accumulating altimeter-derived geostrophic current data, the seasonal variability of the ocean KE has been identified and examined in many regions in the ocean (e.g., Eden and Böning 2002; Jouanno et al. 2012; Rieck et al. 2015; von Appen et al. 2016; Zhai 2017; Kang and Curchitser 2017; Yang and Liang 2018). Figure 11 shows the horizontal distributions of EKE anomalies in the four seasons averaged over the 1994–2015 period. One feature is the spatial inhomogeneity of the EKE seasonality, implying that different mechanisms may at work in different parts of the ocean. For example, the EKE in the WBC regions (e.g., the Kuroshio and Gulf Steam Extensions) peaks in summer and reaches its minimum in winter, which is out of phase with the EKE cycle in the corresponding interior basins.

Figure 12 shows the annual cycles of EKE and the eddy-related canonical transfers (i.e., $\Gamma_K^{0\to3}$, $\Gamma_K^{1\to3}$, and $\Gamma_K^{2\to3}$) averaged over several selected regions. An observation is that both the magnitude and seasonality of $\Gamma_K^{1\to3}$ are generally weaker compared to the other two eddy-related transfers, indicating that KE transfer from the interannual scale is secondary for the seasonal variability of EKE in the ocean. One exception is the Kuroshio Extension region, where the $\Gamma_K^{1\to3}$ has a strong peak in August, which leads the September peak of EKE by one month.

Barotropic instability has been considered as one of the most important mechanisms controlling the seasonal variability of EKE in the ocean (e.g., Eden and Böning 2002; Jouanno et al. 2012). As an indicator for barotropic instability, the canonical transfer of KE from the mean flow to the high-frequency eddies (i.e., $\Gamma_K^{0\to3}$) is found to covary with the EKE seasonal phase in regions
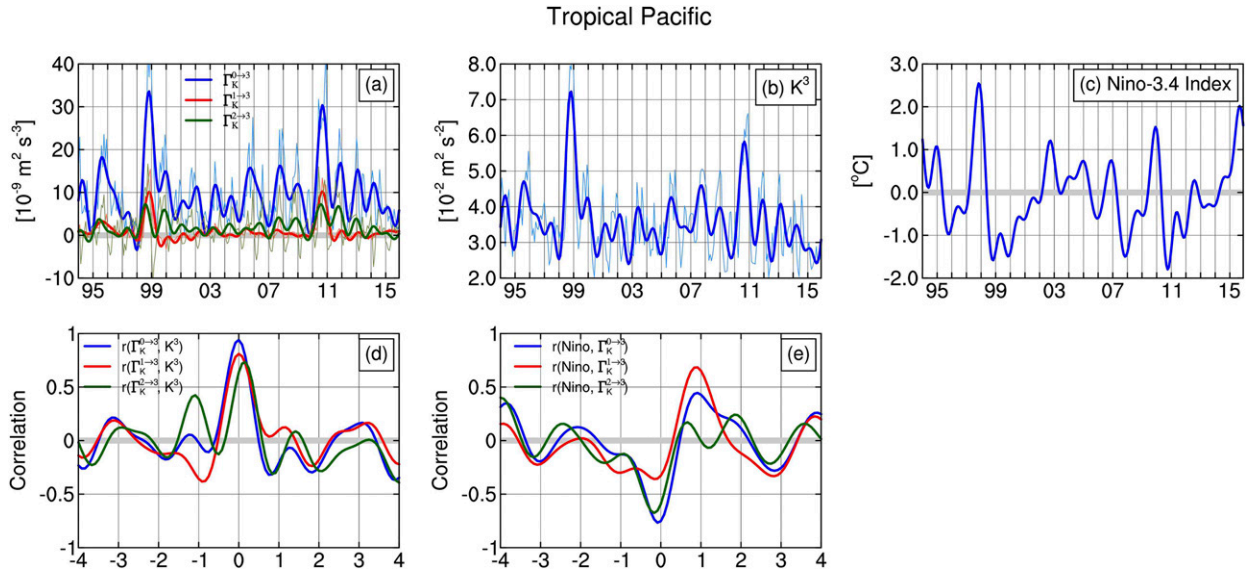
FIG. 9. As in Fig. 8, but for time series of (a) $\Gamma_K^{0\to3}$ (blue line), $\Gamma_K^{1\to3}$ (red line), and $\Gamma_K^{2\to3}$ (green line), (b) K^3 averaged over the tropical Pacific, and (c) the low-pass-filtered Niño-3.4 SST index. (d) Lag correlation between the eddy-related canonical transfers and the K^3 time series. (e) Lag correlation between the Niño-3.4 index and the canonical transfers.

such as the Gulf Stream, the North Pacific subtropical gyre, and the tropical Pacific Ocean (Figs. 12b–d). This indicates that barotropic instability is responsible for the EKE seasonality in these ocean sectors. The annual cycle of the KE transfer from the quasi-annual motions to the high-frequency eddies (i.e., $\Gamma_K^{2\to3}$) reveal some interesting aspects. For instance, it generally peaks 1–2 months before the EKE reaches its maximum (see the green lines in Figs. 12a–d). It is also found that this term is significantly suppressed after the EKE peak and even turns its sign to negative in the following months (Figs. 12a–d). This suggests that the quasi-annual variability provides energy for the growth and development of the high-frequency eddies, and in turn, the eddies transfer energy back to the quasi-annual variability through temporal inverse cascades, analogs to the spatial inverse cascade as identified by previous studies (e.g., Sasaki et al. 2017). In contrast to other regions, the $\Gamma_K^{2\to3}$ averaged in the Southern Ocean exhibits negative values throughout the year and it peaks (negatively) in April–May, which does not correspond to the annual cycle of the EKE that peaks in austral winter. This indicates that other mechanisms, such as wind forcing or baroclinic instability, may explain the EKE seasonality in the Southern Ocean. Note that previous studies based on geostrophic current derived from satellite altimetry found no clear seasonal EKE signals in the Southern Ocean (e.g., Zhai 2017), which is in contrast to the well-defined EKE cycle shown in Fig. 12e. This means that high-frequency ageostrophic motions such as inertial waves, which are not

included in the EKE estimation in the previous studies, contribute mostly to the EKE seasonality in the Southern Ocean. Similar seasonal phase is also observed in the interior basins of the mid-to-high-latitude North Hemisphere.

When averaged over the global ocean, the EKE has a main peak in September–October and a secondary peak in December–January (Fig. 12f). The barotropic transfer $\Gamma_K^{0\to3}$ exhibits a main peak in August and a secondary peak in December–January, which correspond to the two peaks of the EKE seasonal cycle. This suggests that barotropic instability plays an important role in determining the seasonal cycle of EKE in a global integral sense. The seasonal cycle of $\Gamma_K^{2\to3}$ displays a dominant peak in July–September, indicating that the forward KE cascade from the low-frequency quasi-annual motions to the high-frequency eddies is responsible for the September–October peak of the global EKE cycle.

The time-varying canonical KE transfers shown above demonstrate that internal nonlinear processes play crucial roles in determining the temporal variabilities of KEs in different frequency bands. It should be noted that other mechanisms, such as baroclinic instability, wind/buoyancy forcing, nonlocal processes advected from (or to) the remote region, which are not examined in the present study, may also explain the KE characteristics in the ocean. These mechanisms need to be clarified in future studies. Also note that, as a first application of the canonical transfer theory to the global surface currents, here we only give a preliminary report on the temporal variations of the internal energetics
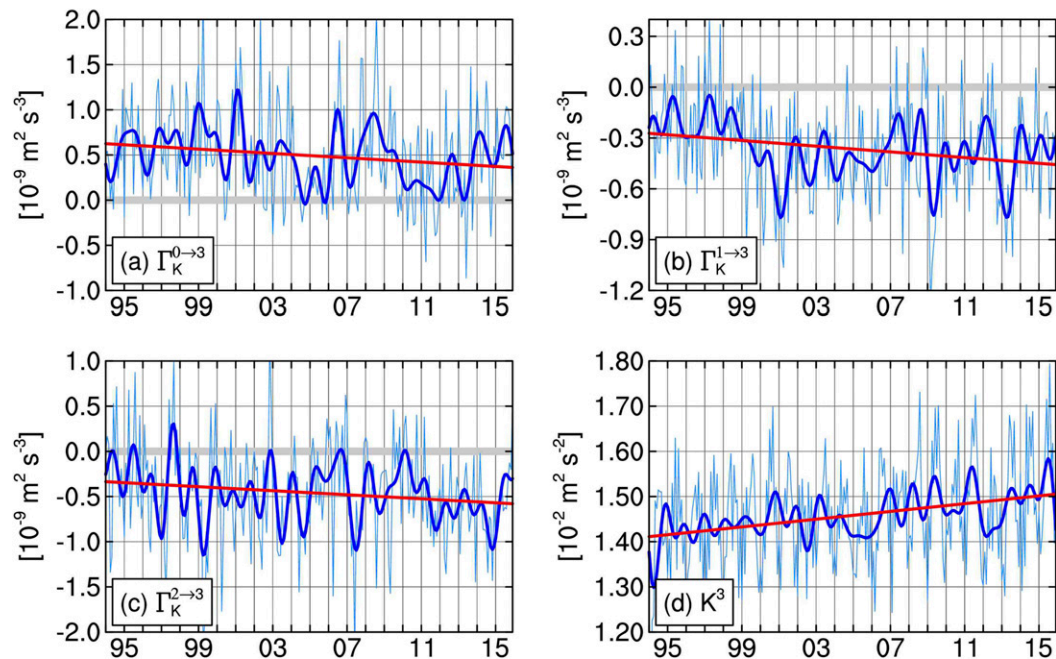
Southern Ocean

FIG. 10. Time series of (a) $\Gamma_K^{0\rightarrow3}$, (b) $\Gamma_K^{1\rightarrow3}$, (c) $\Gamma_K^{2\rightarrow3}$, and (d) K^3 averaged over the Southern Ocean region. Straight red lines denote the linear trends during the period of 1994–2016.

and their relations with some climate modes in several selected regions. The full energetic cycle in each ocean sector should be carefully investigated case by case before a complete story can be reached; we leave that to future studies.

5. Conclusions

Quantifying the interscale energy transfer processes is of fundamental importance in ocean dynamics. In this study, a novel and rigorous canonical transfer theory is employed to characterize the kinetic energy (KE) cascades in the global ocean, using a new surface current synthesis based on satellite observations and an empirical Ekman model. The canonical transfer is distinctly different from the previous formalisms in two aspects. First, by performing a rigorous transport–transfer separation, the canonical transfer gives a faithful representation of the energy cascade among distinct scale windows, which excludes the spatial transport embedded in the nonlinear advection process (Liang 2016). In other words, a canonical transfer is a mere redistribution of energy among the scale windows, without generating or destroying energy as a whole. Second, by taking advantage of a new analysis tool, namely, multiscale window transform (MWT), which is capable of orthogonally decomposing a function space into a direct sum of

several subspaces while retaining the local temporal information in the resulting transform coefficients, the canonical transfer is time dependent, thus allowing us to investigate the temporal variability of the nonlinear multiscale interactions in the ocean.

Four distinct scale windows, namely, the mean flow window, the interannual scale window, the quasi-annual scale window, and the transient eddy window, are considered in this study. The horizontal patterns of the long-term mean canonical transfer matrices demonstrate that multiscale interactions are highly inhomogeneous in the global ocean, with large values concentrated in the WBCs, the Southern Ocean, and the equatorial regions. We found that the temporal inverse KE cascade does not take place everywhere in the ocean. In contrast to the equatorial and WBC regions in which the KE cascades are mainly forward, the Southern Ocean is the very place where coherent large-scale pattern of inverse KE cascade takes place. This suggests that the dynamics of the Southern Ocean might be quite different from that of other strong current regions. In ocean domains such as the WBC regions, the interannual KE mainly comes from the barotropic instability of the mean flow, rather than inverse cascade from high-frequency motions. Even in the Southern Ocean, the contribution to the interannual KE from the mean flow via downscale transfer and that from high-frequency motions via upscale transfer are comparable.
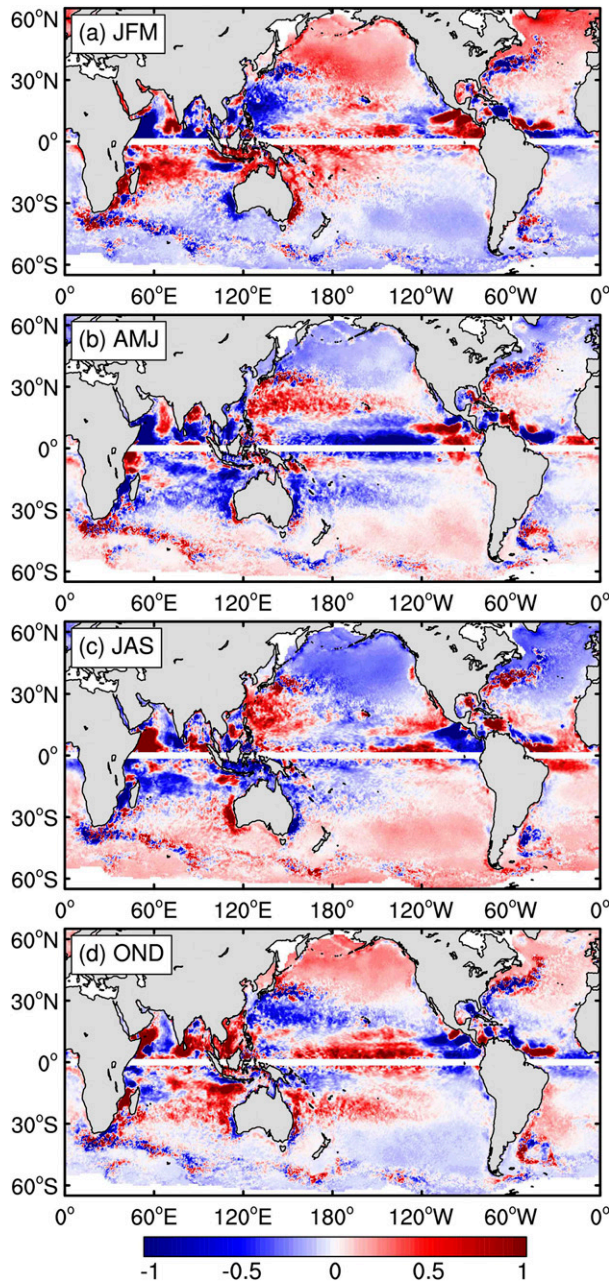
FIG. 11. Seasonal maps of the K^3 anomalies ($10^{-2}\,\mathrm{m^2\,s^{-2}}$) in (a) winter (JFM), (b) spring (AMJ), (c) summer (JAS), and (d) autumn (OND).

Studying the temporal variabilities of the canonical transfers is useful to unravel the time-dependent characteristics of the multiscale ocean energies as well as their relations with the climate system. Strong high-frequency oscillation as well as low-frequency modulation are embedded in the time series of the canonical transfers. Several interesting aspects are found in these feature-rich series. In the Kuroshio Extension region,

the barotropic transfer from the mean flow to the interannual-scale variability largely determines the interannual-scale KE, and is positively correlated with the PDO index at a lag of about 3.5 years, consistent with the scenario of intrinsic variability paced by an external forcing. In the subtropical gyre region, elevated KE transfer from the mean flow to the eddies is observed and is found to be highly correlated with the regional EKE at both interannual and seasonal time scales, suggesting that barotropic instability is also responsible for the local eddy variability, although its contribution might be secondary compared to baroclinic instability as suggested in previous studies (e.g., Chang and Oey 2014). In the tropical region, the downscale transfers to the eddy window from the mean flow, interannual as well as quasi-annual scale windows all contribute to the eddy variability therein, and these transfers are found to decrease (increase) during the El Niño (La Niña) events. In the Southern Ocean, the high-frequency eddies are found to feed KE for the low-frequency variability through temporal inverse cascade processes, and such inverse cascade processes get strengthened due to the enhanced eddy activities in the recent decade. In addition, we also found that, in some regions such as the WBCs and tropical Pacific Ocean, the quasi-annual variability provides energy for the growth and development of the high-frequency eddies, and, in turn, the eddies transfer energy back to the quasi-annual variability through temporal inverse cascades over an annual cycle.

It should be noted that, the present CMEMS current dataset has a relatively coarse resolution, and is only able to resolve eddies with radius longer than about 40 km and lifetime longer than a week due to the interpolation procedure (Chelton et al. 2011). Processes with smaller scales and higher frequencies are largely missing. Their roles in the KE cascade are hence not clear; they can only be determined with higher resolution datasets in the future. Besides, due to the limitation of the satellite observation, this study focuses on the canonical KE transfers in the surface ocean, which is only a part of the complete KE budget. Further questions arise as to how these transfers vary in the vertical direction, and how they are balanced by other processes such as nonlocal transports by advection, pressure work, work done by wind stress, and dissipations.

Given the fact that oceanic mesoscale eddies derive their energy primarily from baroclinic instability, it is desirable to diagnose baroclinic instabilities, which are however missing in this study due to a lack of necessary information for density in the satellite observation. As established in Liang (2016), baroclinic instability is measured by the canonical transfer of available potential energy, which requires knowledge of both density and velocity fields (vertical information is also needed to
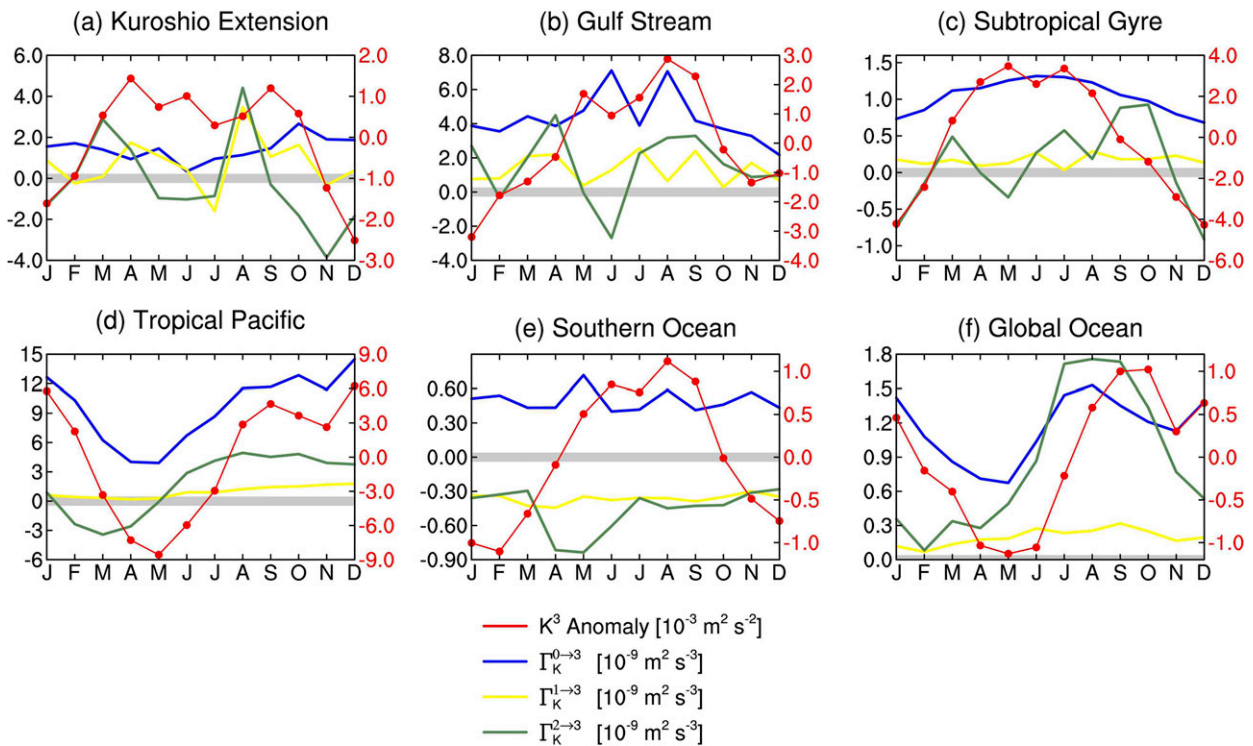
FIG. 12. The seasonal cycle of the K^3 anomalies (red), $\Gamma_K^{0 \to 3}$ (blue), $\Gamma_K^{1 \to 3}$ (yellow), and $\Gamma_K^{2 \to 3}$ (green) in the (a) Kuroshio Extension, (b) Gulf Stream, (c) the North Pacific subtropical gyre, (d) tropical Pacific, (e) Southern Ocean, and (f) the global ocean. The K^3 anomalies are in $10^{-2} \, m^2 \, s^{-2}$ and canonical transfers are in $10^{-9} \, m^2 \, s^{-3}$.

determine the stratification). We have to leave the spatiotemporal structure of the baroclinic canonical transfer, and hence baroclinic instabilities, to future studies.

REFERENCES

Aluie, H., M. Hecht, and G. K. Vallis, 2018: Mapping the energy cascade in the North Atlantic Ocean: The coarse-graining approach. *J. Phys. Oceanogr.*, **48**, 225–244, https://doi.org/10.1175/JPO-D-17-0100.1.

Arbic, B. K., R. B. Scott, G. R. Flierl, A. J. Morten, J. G. Richman, and J. F. Shriver, 2012: Nonlinear cascades of surface oceanic geostrophic kinetic energy in the frequency domain. *J. Phys. Oceanogr.*, **42**, 1577–1600, https://doi.org/10.1175/JPO-D-11-0151.1.

——, M. Müller, J. G. Richman, J. F. Shriver, A. J. Morten, R. B. Scott, G. Sérazin, and T. Penduff, 2014: Geostrophic turbulence in the frequency–wavenumber domain: Eddy-driven low-frequency variability. *J. Phys. Oceanogr.*, **44**, 2050–2069, https://doi.org/10.1175/JPO-D-13-054.1.

Berloff, P., A. M. C. Hogg, and W. Dewar, 2007: The turbulent oscillator: A mechanism of low-frequency variability of the wind-driven ocean gyres. *J. Phys. Oceanogr.*, **37**, 2363–2386, https://doi.org/10.1175/JPO3118.1.

Capet, X., J. C. McWilliams, M. J. Molemaker, and A. F. Shchepetkin, 2008: Mesoscale to submesoscale transition in the California Current System. Part III: Energy balance and flux. *J. Phys. Oceanogr.*, **38**, 2256–2269, https://doi.org/10.1175/2008JPO3810.1.

Chang, Y.-L., and L.-Y. Oey, 2014: Instability of the North Pacific Subtropical Countercurrent. *J. Phys. Oceanogr.*, **44**, 818–833, https://doi.org/10.1175/JPO-D-13-0162.1.

Charney, J. G., 1971: Geostrophic turbulence. *J. Atmos. Sci.*, **28**, 1087–1095, https://doi.org/10.1175/1520-0469(1971)028<1087:GT>2.0.CO;2.

Chelton, D. B., M. G. Schlax, and R. M. Samelson, 2011: Global observations of nonlinear mesoscale eddies. *Prog. Oceanogr.*, **91**, 167–216, https://doi.org/10.1016/j.pocean.2011.01.002.

Eden, C., and C. Böning, 2002: Sources of eddy kinetic energy in the Labrador Sea. *J. Phys. Oceanogr.*, **32**, 3346–3363, https://doi.org/10.1175/1520-0485(2002)032<3346:SOEKEI>2.0.CO;2.

——, L. Czeschel, and D. Olbers, 2014: Toward energetically consistent ocean models. *J. Phys. Oceanogr.*, **44**, 3160–3184, https://doi.org/10.1175/JPO-D-13-0260.1.

Ferrari, R., and C. Wunsch, 2009: Ocean circulation kinetic energy: Reservoirs, sources, and sinks. *Annu. Rev. Fluid Mech.*, **41**, 253–282, https://doi.org/10.1146/annurev.fluid.40.111406.102139.

Hogg, A. McC., M. P. Meredith, D. P. Chambers, E. P. Abrahamsen, C. W. Hughes, and A. K. Morrison, 2015: Recent trends in the Southern Ocean eddy field. *J. Geophys. Res. Oceans*, **120**, 257–267, https://doi.org/10.1002/2014JC010470.

Holopainen, E. O., 1978: A diagnostic study of the kinetic energy balance of the long-term mean flow and the associated transient fluctuations in the atmosphere. *Geophysica*, **15**, 125–145.

Jouanno, J., J. Sheinbaum, B. Barnier, J. M. Molines, and J. Candela, 2012: Seasonal and interannual modulation of the eddy kinetic energy in the Caribbean Sea. *J. Phys. Oceanogr.*, **42**, 2041–2055, https://doi.org/10.1175/JPO-D-12-048.1.

Kang, D., and E. N. Curchitser, 2017: On the evaluation of seasonal variability of the ocean kinetic energy. *J. Phys. Oceanogr.*, **47**, 1675–1683, https://doi.org/10.1175/JPO-D-17-0063.1.

Khatri, H., J. Sukhatme, A. Kumar, and M. K. Verma, 2018: Surface ocean enstrophy, kinetic energy fluxes, and spectra from satellite altimetry. *J. Geophys. Res. C Oceans*, **123**, 3875–3892, https://doi.org/10.1029/2017JC013516.

Klein, P., B. L. Hua, G. Lapeyre, X. Capet, S. Le Gentil, and H. Sasaki, 2008: Upper ocean turbulence from high-resolution 3D simulations. *J. Phys. Oceanogr.*, **38**, 1748–1763, https://doi.org/10.1175/2007JPO3773.1.

Kobashi, F., and H. Kawamura, 2002: Seasonal variation and instability nature of the North Pacific Subtropical Countercurrent and the Hawaiian Lee Countercurrent. *J. Geophys. Res. Oceans*, **107**, 3185, https://doi.org/10.1029/2001JC001225.

Li, L., A. P. Ingersoll, X. Jiang, D. Feldman, and Y. L. Yung, 2007: Lorenz energy cycle of the global atmosphere based on reanalysis datasets. *Geophys. Res. Lett.*, **34**, L16813, https://doi.org/10.1029/2007GL029985.

Liang, X. S., 2016: Canonical transfer and multiscale energetics for primitive and quasigeostrophic atmospheres. *J. Atmos. Sci.*, **73**, 4439–4468, https://doi.org/10.1175/JAS-D-16-0131.1.

——, and A. R. Robinson, 2005: Localized multiscale energy and vorticity analysis: I. Fundamentals. *Dyn. Atmos. Oceans*, **38**, 195–230, https://doi.org/10.1016/j.dynatmoce.2004.12.004.

——, and D. G. M. Anderson, 2007: Multiscale window transform. *Multiscale Model. Simul.*, **6**, 437–467, https://doi.org/10.1137/06066895X.

——, and A. R. Robinson, 2007: Localized multi-scale energy and vorticity analysis: II. Finite-amplitude instability theory and validation. *Dyn. Atmos. Oceans*, **44**, 51–76, https://doi.org/10.1016/j.dynatmoce.2007.04.001.

Lorenz, E. N., 1955: Available potential energy and the maintenance of the general circulation. *Tellus*, **7**, 157–167, https://doi.org/10.3402/tellusa.v7i2.8796.

Meredith, M. P., and A. M. Hogg, 2006: Circumpolar response of Southern Ocean eddy activity to a change in the Southern Annular Mode. *Geophys. Res. Lett.*, **33**, L16608, https://doi.org/10.1029/2006GL026499.

O'Rourke, A. K., B. K. Arbic, and S. M. Griffies, 2018: Frequency-domain analysis of atmospherically forced versus intrinsic ocean surface kinetic energy variability in GFDL's CM2-O model hierarchy. *J. Climate*, **31**, 1789–1810, https://doi.org/10.1175/JCLI-D-17-0024.1.

Pan, Y., L. Li, X. Jiang, G. Li, W. Zhang, X. Wang, and A. P. Ingersoll, 2017: Earth's changing global atmospheric energy cycle in response to climate change. *Nat. Commun.*, **8**, 14 367, https://doi.org/10.1038/ncomms14367.

Pedlosky, J., 1987: *Geophysical Fluid Dynamics*. 2nd ed. Springer-Verlag, 710 pp.

Penduff, T., M. Juza, L. Brodeau, G. C. Smith, B. Barnier, J.-M. Molines, A.-M. Treguier, and G. Madec, 2010: Impact of global ocean model resolution on sea-level variability with emphasis on interannual time scales. *Ocean Sci.*, **6**, 269–284, https://doi.org/10.5194/os-6-269-2010.

——, ——, B. Barnier, J. Zika, W. K. Dewar, A.-M. Treguier, J.-M. Molines, and N. Audiffren, 2011: Sea level expression of intrinsic and forced ocean variabilities at interannual time scales. *J. Climate*, **24**, 5652–5670, https://doi.org/10.1175/JCLI-D-11-00077.1.

Pierini, S., 2014: Kuroshio extension bimodality and the North Pacific Oscillation: A case of intrinsic variability paced by external forcing. *J. Climate*, **27**, 448–454, https://doi.org/10.1175/JCLI-D-13-00306.1.

Plumb, R. A., 1983: A new look at the energy cycle. *J. Atmos. Sci.*, **40**, 1669–1688, https://doi.org/10.1175/1520-0469(1983)040<1669:ANLATE>2.0.CO;2.

Pujol, M.-I., Y. Faugère, G. Taburet, S. Dupuy, C. Pelloquin, M. Ablain, and N. Picot, 2016: DUACS DT2014: The new multi-mission altimeter data set reprocessed over 20 years. *Ocean Sci.*, **12**, 1067–1090, https://doi.org/10.5194/os-12-1067-2016.

Qiu, B., 2003: Kuroshio extension variability and forcing of the pacific decadal oscillations: Responses and potential feedback. *J. Phys. Oceanogr.*, **33**, 2465–2482, https://doi.org/10.1175/2459.1.

——, and S. Chen, 2013: Concurrent decadal mesoscale eddy modulations in the western North Pacific Subtropical Gyre. *J. Phys. Oceanogr.*, **43**, 344–358, https://doi.org/10.1175/JPO-D-12-0133.1.

Rieck, J. K., C. W. Böning, R. J. Greatbatch, and M. Scheinert, 2015: Seasonal variability of eddy kinetic energy in a global high-resolution ocean model. *Geophys. Res. Lett.*, **42**, 9379–9386, https://doi.org/10.1002/2015GL066152.

Rio, M.-H., S. Mulet, and N. Picot, 2014: Beyond GOCE for the ocean circulation estimate: Synergetic use of altimetry, gravimetry, and in situ data provides new insight into geostrophic and Ekman currents. *Geophys. Res. Lett.*, **41**, 8918–8925, https://doi.org/10.1002/2014GL061773.

Salmon, R., 1980: Baroclinic instability and geostrophic turbulence. *Geophys. Astrophys. Fluid Dyn.*, **15**, 167–211, https://doi.org/10.1080/03091928008241178.

Saltzman, B., 1957: Equations governing the energetics of the larger scales of atmospheric turbulence in the domain of wave number. *J. Meteor.*, **14**, 513–523, https://doi.org/10.1175/1520-0469(1957)014<0513:EGTEOT>2.0.CO;2.

Sasaki, H., P. Klein, Y. Sasai, and B. Qiu, 2017: Regionality and seasonality of submesoscale and mesoscale turbulence in the North Pacific Ocean. *Ocean Dyn.*, **67**, 1195–1216, https://doi.org/10.1007/s10236-017-1083-y.

Schlösser, F., and C. Eden, 2007: Diagnosing the energy cascade in a model of the North Atlantic. *Geophys. Res. Lett.*, **34**, L02604, https://doi.org/10.1029/2006GL027813.

Scott, R. B., and F. Wang, 2005: Direct evidence of an oceanic inverse kinetic energy cascade from satellite altimetry. *J. Phys. Oceanogr.*, **35**, 1650–1666, https://doi.org/10.1175/JPO2771.1.

——, and B. K. Arbic, 2007: Spectral energy fluxes in geostrophic turbulence: Implications for ocean energetics. *J. Phys. Oceanogr.*, **37**, 673–688, https://doi.org/10.1175/JPO3027.1.

Sérazin, G., T. Penduff, B. Barnier, J.-M. Molines, B. K. Arbic, M. Müller, and L. Terray, 2018: Inverse cascades of kinetic

energy as a source of intrinsic variability: A global OGCM study. *J. Phys. Oceanogr.*, **48**, 1385–1408, https://doi.org/10.1175/JPO-D-17-0136.1.

Stammer, D., and C. Wunsch, 1999: Temporal changes in eddy energy of the oceans. *Deep-Sea Res. II*, **46**, 77–108, https://doi.org/10.1016/S0967-0645(98)00106-4.

Strang, G., and T. Nguyen, 1996: *Wavelets and Filter Banks*. 2nd ed. Wellesley-Cambridge Press, 520 pp.

Taguchi, B., S.-P. Xie, N. Schneider, M. Nonaka, H. Sasaki, and Y. Sasai, 2007: Decadal variability of the Kuroshio Extension: Observations and an eddy-resolving model hindcast. *J. Climate*, **20**, 2357–2377, https://doi.org/10.1175/JCLI4142.1.

Taylor, G. I., 1938: The spectrum of turbulence. *Proc. Roy. Soc. London*, **A164**, 476–490, https://doi.org/10.1098/rspa.1938.0032.

Tulloch, R., J. Marshall, C. Hill, and K. S. Smith, 2011: Scales, growth rates, and spectral fluxes of baroclinic instability in the ocean. *J. Phys. Oceanogr.*, **41**, 1057–1076, https://doi.org/10.1175/2011JPO4404.1.

Venaille, A., G. K. Vallis, and K. S. Smith, 2011: Baroclinic turbulence in the ocean: analysis with primitive equation and quasigeostrophic simulations. *J. Phys. Oceanogr.*, **41**, 1605–1623, https://doi.org/10.1175/JPO-D-10-05021.1.

von Appen, W.-J., U. Schauer, T. Hattermann, and A. Beszczynska-Möller, 2016: Seasonal cycle of mesoscale instability of the West Spitsbergen Current. *J. Phys. Oceanogr.*, **46**, 1231–1254, https://doi.org/10.1175/JPO-D-15-0184.1.

von Storch, J.-S., C. Eden, I. Fast, H. Haak, D. Hernández-Deckers, E. Maier-Reimer, J. Marotzke, and D. Stammer, 2012: An estimate of the Lorenz energy cycle for the World Ocean based on the STORM/NCEP simulation. *J. Phys. Oceanogr.*, **42**, 2185–2205, https://doi.org/10.1175/JPO-D-12-079.1.

Wang, S., Z. Liu, and C. Pang, 2015: Geographical distribution and anisotropy of the inverse kinetic energy cascade, and its role in the eddy equilibrium processes. *J. Geophys. Res. Oceans*, **120**, 4891–4906, https://doi.org/10.1002/2014JC010476.

Wilkin, J. L., and R. A. Morrow, 1994: Eddy kinetic energy and momentum flux in the Southern Ocean: Comparison of a global eddy-resolving model with altimeter, drifter, and current-meter data. *J. Geophys. Res. Oceans*, **99**, 7903–7916, https://doi.org/10.1029/93JC03505.

Williams, R. G., C. Wilson, and C. W. Hughes, 2007: Ocean and atmosphere storm tracks: The role of eddy vorticity forcing. *J. Phys. Oceanogr.*, **37**, 2267–2289, https://doi.org/10.1175/JPO3120.1.

Yang, Y., and X. S. Liang, 2016: The instabilities and multiscale energetics underlying the mean–interannual–eddy interactions in the Kuroshio Extension region. *J. Phys. Oceanogr.*, **46**, 1477–1494, https://doi.org/10.1175/JPO-D-15-0226.1.

——, and ——, 2018: On the seasonal eddy variability in the Kuroshio Extension. *J. Phys. Oceanogr.*, **48**, 1675–1689, https://doi.org/10.1175/JPO-D-18-0058.1.

——, ——, B. Qiu, and S. Chen, 2017: On the decadal variability of the eddy kinetic energy in the Kuroshio Extension. *J. Phys. Oceanogr.*, **47**, 1169–1187, https://doi.org/10.1175/JPO-D-16-0201.1.

Youngs, M. K., A. F. Thompson, A. Lazar, and K. J. Richards, 2017: ACC meanders, energy transfer, and mixed barotropic–baroclinic instability. *J. Phys. Oceanogr.*, **47**, 1291–1305, https://doi.org/10.1175/JPO-D-16-0160.1.

Zemskova, V. E., B. L. White, and A. Scotti, 2015: Available potential energy and the general circulation: Partitioning wind, buoyancy forcing, and diapycnal mixing. *J. Phys. Oceanogr.*, **45**, 1510–1531, https://doi.org/10.1175/JPO-D-14-0043.1.

Zhai, X., 2017: The annual cycle of surface eddy kinetic energy and its influence on eddy momentum fluxes as inferred from altimeter data. *Satell. Oceanogr. Meteor.*, **2**, 299, https://doi.org/10.18063/som.v2i2.299.

Zheng, S., M. Feng, Y. Du, X. Cheng, and J. Li, 2016: Annual and interannual variability of the tropical instability vortices in the equatorial eastern Pacific observed from Lagrangian surface drifters. *J. Climate*, **29**, 9163–9177, https://doi.org/10.1175/JCLI-D-16-0124.1.